Morphological image analysis

Michielsen, K.F L; de Raedt, H.A.

Published in:
Computer Physics Communications

DOI:
10.1016/S0010-4655(00)00139-9

Publication date:
2000

Computer Physics Communications 132 (2000) 94–103

Computer Physics Communications

www.elsevier.nl/locate/cpc

Morphological image analysis

K. Michielsen [a], H. De Raedt [b,*]

[a] *Laboratory for Biophysical Chemistry, University of Groningen, Nijenborgh 4, NL-9747 AG Groningen, The Netherlands*
[b] *Institute for Theoretical Physics and Materials Science Centre, University of Groningen, Nijenborgh 4, NL-9747 AG Groningen, The Netherlands*

Received 24 November 1999; received in revised form 31 March 2000

Abstract

We describe a morphological image analysis method to characterize black-and-white images in terms of geometry and topology by means of the Minkowski functionals. We present an algorithm to calculate these functionals in two and three dimensions and apply the method to random point patterns on square and cubic lattices.

Keywords: Integral geometry; Minkowski functionals; Geometry and topology; Euler characteristic; Random point sets

1. Introduction

Image analysis is important for many applications in science and engineering. For example, the interpretation of images taken by satellites, medical imaging tools (e.g., X-ray tomography, magnetic resonance imaging), and microscopes involves some kind of image processing, some being much more sophisticated than others. In the case of (electron) microscope images of materials such as polymer mixtures and ceramics, the main purpose of image analysis is to provide a quantitative characterization of the shape, structure and connectivity of the constituents. The purpose of this paper is to describe an easy-to-use, versatile method to compute the morphological properties of such images.

In general images are represented by (a set of) intensities at each point of the image, the intensities being continuous functions of the position. In practice these images often come in digitized form. Digitizing an image [1] maps the position within the image onto a grid and attaches to each cell of the grid quantized values of the intensities. The latter are usually determined by first dividing the intensity range into a fixed number of bins and assigning to each cell the number of the bin that most closely matches the intensity. The most extreme form of quantization, using only two bins, yields black-and-white images [1].

Morphological image analysis (MIA) characterizes black-and-white images in terms of shape (geometry) and connectivity (topology) by means of the Minkowski functionals known from integral geometry [2–4]. These functionals are related to familiar measures: In two (three) dimensions they correspond to the covered area,

* Corresponding author.
E-mail addresses: deraedt@phys.rug.nl (H. De Raedt), K.F.L.Michielsen@chem.rug.nl (K. Michielsen).

0010-4655/00/$ – see front matter
PII: S0010-4655(00)00139-9

boundary length, and connectivity (volume, surface area, integral mean curvature and connectivity) of the pattern. For sufficiently smooth and regular objects some of these measures are related to quantities known from differential geometry. Integral geometry imposes no limitations on the properties of the patterns. Furthermore in integral geometry the calculation of the Minkowski functionals is relatively straightforward and requires little computational effort.

Given a set of patterns the first step in MIA is to compute the Minkowski functionals themselves. The second step is to analyze the behavior of the Minkowski functionals as a function of one or more control parameters. This approach has proven to be very useful to describe the morphology of porous media and complex fluids, the large-scale distribution of matter in the Universe, microemulsions, patterns in reaction diffusion systems, and spinodal decomposition kinetics [5].

In this paper we first describe an algorithm to calculate the Minkowski functionals for two and three-dimensional black-and-white digitized images. We then illustrate the application of MIA to two and three-dimensional random patterns and show that there is excellent agreement with analytical results.

2. Morphological properties

We consider a two-dimensional (2D) [three-dimensional (3D)] black-and-white image projected on a grid $\mathcal{G}$. Each square (cube) is centered at a lattice point $\mathbf{x} \in \mathcal{G}$ and is called a pixel (voxel). Since the output of image analysis should be the description of a given picture we have to define the various objects building up the picture [1]. This is done as follows:

$$\mathcal{P}(\mathbf{x}) = \begin{cases} 1 & \text{if } \mathbf{x} \text{ belongs to an object,} \\ 0 & \text{if } \mathbf{x} \text{ belongs to the background,} \end{cases} \tag{1}$$

where $\mathcal{P}(\mathbf{x}) = 0$ corresponds to a white pixel and $\mathcal{P}(\mathbf{x}) = 1$ to a black pixel.

According to integral geometry, the morphological properties of the various objects building up the black-and-white picture can be completely described in terms of Minkowski functionals [2]. In two dimensions ($d = 2$) [three dimensions ($d = 3$)] the Minkowski functionals are proportional to the area $A^{(d=2)}$ covered by the black pixels, the boundary length L and the Euler characteristic or connectivity number $\chi^{(d=2)}$ (volume V, surface area $A^{(d=3)}$, integral mean curvature H and $\chi^{(d=3)}$). In differential geometry the integral mean curvature H is defined as $\int \mathrm{d}f(R_1 + R_2)/2R_1R_2$, where R_1 and R_2 are the principal radii of curvature of the surface and $\mathrm{d}f$ is the area element. In 3D the Euler characteristic is related to the integral Gaussian curvature, defined as $G = \int \mathrm{d}f(1/R_1R_2)$. The functional $\chi^{(d)}$ as defined in integral geometry is the same as the Euler characteristic defined in algebraic topology [2]: $\chi^{(d=2)}$ equals the number of connected components minus the number of holes and $\chi^{(d=3)}$ is given by the number of connected components minus the number of tunnels (torus-like holes) plus the number of cavities. For example, $\chi^{(d=3)} = 1$ for a solid cube, $\chi^{(d=3)} = 2$ for a hollow cube and $\chi^{(d=3)} = 0$ for a cube pierced by a tunnel. The Euler characteristic is negative for multiply connected structures. For complex structures it is often difficult to identify the number of connected components, tunnels and cavities. However, integral-geometry-based MIA directly yields $\chi^{(d)}$.

Table 1
Morphological properties for the open elements Q_ν ($\nu = 0, \ldots, d = 2$), the basic building blocks of a two-dimensional square lattice. Q_0: vertex; Q_1: open line segment of length a; Q_2: open square of edge length a. $A^{(d=2)}$ denotes the covered area, L the boundary length and $\chi^{(d=2)}$ the Euler characteristic

	$A^{(d=2)}$	L	$\chi^{(d=2)}$
Q_2	a^2	$-4a$	1
Q_1	0	$2a$	-1
Q_0	0	0	1

Table 2
Morphological properties for the open elements Q_ν ($\nu = 0, \ldots, d = 3$), the basic building blocks of a three-dimensional cubic lattice. Q_0: vertex; Q_1: open line segment of length a; Q_2: open square of edge length a; Q_3: open cube of edge length a. V denotes the volume, $A^{(d=3)}$ the surface area, H the integral mean curvature and $\chi^{(d=3)}$ the Euler characteristic

	V	$A^{(d=3)}$	H	$\chi^{(d=3)}$
Q_3	a^3	$-6a^2$	$3\pi a$	-1
Q_2	0	$2a^2$	$-2\pi a$	1
Q_1	0	0	πa	-1
Q_0	0	0	0	1

In order to calculate the morphological properties of $\mathcal{P}(\mathbf{x})$ in an efficient way we consider each pixel (voxel) as the union of the disjoint collection of its interior, faces (for the 3D case only), open edges and vertices. On a square and cubic lattice there are $d+1$ of these open elements Q_ν, $\nu = 0, \ldots, d$: Q_0 corresponds to a vertex, Q_1 to an open line segment, Q_2 to an open square on both the 2D square and 3D cubic lattice, and Q_3 to an open cube on the 3D cubic lattice. The values of V, $A^{(d)}$, L, H and $\chi^{(d)}$ for the building blocks Q_ν of a 2D square and a 3D cubic lattice can easily be calculated [6] and are listed in Tables 1 and 2, respectively. For the whole image $\mathcal{P} = \mathcal{P}(\mathbf{x})$ these functionals can be calculated using

$$Y(\mathcal{P}) = \sum_{\nu=0}^{d} Y(Q_\nu) n_\nu(\mathcal{P}), \tag{2}$$

where $n_\nu(\mathcal{P})$ denotes the number of open elements Q_ν present in $\mathcal{P}$ and in 2D (3D) Y stands for $A^{(d=2)}$, L, and $\chi^{(d=2)}$ (V, $A^{(d=3)}$, H, and $\chi^{(d=3)}$), respectively.

2.1. Two-dimensional images

We now describe a procedure to determine how the number of open bodies of each type changes when one adds (removes) one black pixel to (from) a given 2D pattern $\mathcal{P}(\mathbf{x}) = \mathcal{P}(i, j)$ for $i = 1, \ldots, L_x$ and $j = 1, \ldots, L_y$. Using this procedure it is easy to compute the Minkowski functionals for a given pattern, simply by adding the black pixels one-by-one to an initially complete white background.

Obviously, the number $n_2(\mathcal{P})$ of open squares building up the black objects on the $L_x \times L_y$ picture $\mathcal{P}(\mathbf{x})$ increases (decreases) with one if one adds (removes) one black pixel at the position $\mathbf{x} = (i, j)$ to (from) the image. Therefore if we add a black pixel

$$\Delta n_2(\mathcal{P}) = 1, \tag{3}$$

where we introduce the symbol Δ to indicate that we compute the difference resulting from adding one black pixel.

Similarly the change in the number of open line segments, $\Delta n_1(\mathcal{P})$ is given by

$$\Delta n_1(\mathcal{P}) = \sum_{\alpha=\pm 1} \big[\mathcal{Q}(i+\alpha, j) + \mathcal{Q}(i, j+\alpha)\big], \tag{4}$$

where $\mathcal{Q}(\mathbf{x}) \equiv 1 - \mathcal{P}(\mathbf{x})$. Finally the change in the number of vertices, $n_0(\mathcal{P})$ reads

$$\Delta n_0(\mathcal{P}) = \sum_{\alpha,\beta=\pm 1} \mathcal{Q}(i+\alpha, j)\mathcal{Q}(i+\alpha, j+\beta)\mathcal{Q}(i, j+\beta). \tag{5}$$

By stepping through the 2D grid, adding black pixels one at a time and computing the changes Δn_0, Δn_1, and Δn_2, we easily obtain the three Minkowski functionals.

2.2. Three-dimensional images

The procedure for 3D images [$\mathcal{P}(\mathbf{x}) = \mathcal{P}(i, j, k)$ for $i = 1, \ldots, L_x$, $j = 1, \ldots, L_y$ and $k = 1, \ldots, L_z$] is almost identical to the one described above. We find

$$\Delta n_3(\mathcal{P}) = 1, \tag{6}$$

for the change in the number of open cubes,

$$\Delta n_2(\mathcal{P}) = \sum_{\alpha=\pm 1} \big[\mathcal{Q}(i+\alpha, j, k) + \mathcal{Q}(i, j+\alpha, k) + \mathcal{Q}(i, j, k+\alpha)\big], \tag{7}$$

for the change in the number of open squares,

$$\begin{aligned}\Delta n_1(\mathcal{P}) = \sum_{\alpha,\beta=\pm 1} \big[& \mathcal{Q}(i+\alpha, j, k)\mathcal{Q}(i+\alpha, j+\beta, k)\mathcal{Q}(i, j+\beta, k) \\ & + \mathcal{Q}(i, j+\alpha, k)\mathcal{Q}(i, j+\alpha, k+\beta)\mathcal{Q}(i, j, k+\beta) \\ & + \mathcal{Q}(i+\alpha, j, k)\mathcal{Q}(i+\alpha, j, k+\beta)\mathcal{Q}(i, j, k+\beta)\big],\end{aligned} \tag{8}$$

for the change in the number of open line segments, and

$$\begin{aligned}\Delta n_0(\mathcal{P}) = \sum_{\alpha,\beta,\gamma=\pm 1} & \mathcal{Q}(i+\alpha, j, k)\mathcal{Q}(i+\alpha, j+\beta, k)\mathcal{Q}(i, j+\beta, k) \\ & \times \mathcal{Q}(i+\alpha, j, k+\gamma)\mathcal{Q}(i+\alpha, j+\beta, k+\gamma) \\ & \times \mathcal{Q}(i, j+\beta, k+\gamma)\mathcal{Q}(i, j, k+\gamma),\end{aligned} \tag{9}$$

for the change in the number of vertices.

In Appendix A we give an example of a computer code that computes $\Delta n_v(\mathcal{P})$ for a 3D rectangular lattice with free boundary conditions. It is obvious that it is very compact and requires little computation per grid point.

2.3. Illustrative example

As a simple example we calculate the Minkowski functionals for the 2D checkerboard pattern with an even number $L_x = L_y$ of cells, of edge length $a = 1$, in each direction. We consider free and periodic boundary conditions. An illustration is given in Fig. 1. The left panel in Fig. 1 shows the 4×4 checkerboard lattice with free boundary conditions, i.e. the pattern is completely surrounded by white pixels. The right panel shows the same pattern but with periodic boundary conditions. For the $L_x \times L_x$ checkerboard $\mathcal{P}_F$ with free boundary conditions we find $n_0(\mathcal{P}_F) = (L_x + 1)^2 - 2$, $n_1(\mathcal{P}_F) = 2L_x^2$, $n_2(\mathcal{P}_F) = L_x^2/2$ and hence $A^{(d=2)}(\mathcal{P}_F) = L_x^2/2$, $L(\mathcal{P}_F) = 2L_x^2$ and $\chi^{(d=2)}(\mathcal{P}_F) = L_x^2/2 - (L_x - 1)^2$. Note that this value of $\chi^{(d=2)}$ corresponds to the value we find if we calculate $\chi^{(d=2)}$ as the number of connected components minus the number of holes, since the number of connected components (black structure) equals one and the number of holes equals $(L_x/2 - 1)(L_x - 2)$. For the $L_x \times L_x$ checkerboard $\mathcal{P}_P$ with periodic boundary conditions we find $n_0(\mathcal{P}_P) = L_x^2$, $n_1(\mathcal{P}_P) = 2L_x^2$, $n_2(\mathcal{P}_P) = L_x^2/2$ which yields $A^{(d=2)}(\mathcal{P}_P) = L_x^2/2$, $L(\mathcal{P}_P) = 2L_x^2$ and $\chi^{(d=2)}(\mathcal{P}_P) = -L_x^2/2$. Note that $\chi^{(d=2)}(\mathcal{P}_P)/L_x^2 = \lim_{L_x\to\infty} \chi^{(d=2)}(\mathcal{P}_F)/L_x^2 = -1/2$.

3. Application: Random point patterns

Many systems observed in nature may be modeled by point patterns. For example, a system of particles may be viewed as a system of points generated by the centres of the particles. Point systems may be considered as black-and-white pictures. Single black pixels (voxels) represent the germs of the model [4,7]. In order to study the

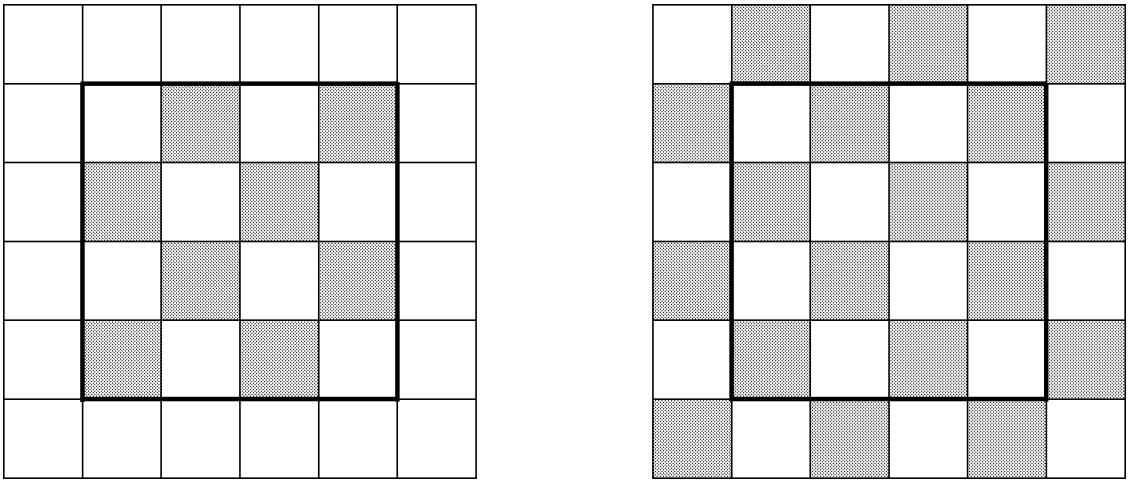

Fig. 1. 4×4 checkerboard pattern. The black line denotes the boundary. Left: free boundaries; right: periodic boundaries. In MIA all dark pixels are considered to be black.

characteristics (degree of randomness, clustering, periodic ordering, ...) of the point system on a square (cubic) lattice we attach squares (cubes) to each point. These squares (cubes) are called the grains [4,7] of the model and are constructed as follows: We consider the germs to be squares (cubes) of edge length $r = 1$ and the grains as enlarged squares (cubes) of edge length $2r + 1$, $r \geqslant 0$. The graining procedure is demonstrated in Fig. 2 for two dimensions. The study of the coverage of the image by the grains gives information about the system under investigation.

We consider a collection of N pixels (voxels) p_i in a square (cubic) domain $\Omega \subset \mathcal{G}$ of volume $|\Omega| = L_x^2$ (L_x^3). The positions of the pixels (voxels) are generated from a uniformly uncorrelated random distribution. The mean density of pixels (voxels) equals $\rho = N/|\Omega|$. We attach to every germ p_i a square (cubic) grain C_i of edge length a. In the bulk limit N, $\Omega \to \infty$ with ρ fixed, the averages of the morphological quantities of the ensemble of configurations of the square (cubic) grains C_i with density ρ read in three dimensions [6]

$$\langle V/N \rangle = (1 - \mathrm{e}^{-n})/\rho, \tag{10a}$$

$$\langle A^{(d=3)}/N \rangle = 6a^2\mathrm{e}^{-n}, \tag{10b}$$

$$\langle H/N \rangle = 3\pi a(1-n)\mathrm{e}^{-n}, \tag{10c}$$

$$\langle \chi^{(d=3)}/N \rangle = (1 - 3n + n^2)\mathrm{e}^{-n}, \tag{10d}$$

with $n = \rho a^3$ and $a = 2r + 1$, $r \geqslant 0$, and in two dimensions

$$\langle A^{(d=2)}/N \rangle = (1 - \mathrm{e}^{-n})/\rho, \tag{11a}$$

$$\langle L/N \rangle = 4a\mathrm{e}^{-n}, \tag{11b}$$

$$\langle \chi^{(d=2)}/N \rangle = (1-n)\mathrm{e}^{-n}, \tag{11c}$$

with $n = \rho a^2$ and $a = 2r + 1$, $r \geqslant 0$.

We will now study the morphological quantities for sets of points which are randomly positioned in a square (cube) of edge length L_x. By making use of the graining procedure described above we transform the point pattern into a pattern of square (cubic) grains of edge length $a = 2r + 1$, $r \geqslant 0$ and study the behavior of the morphological quantities as a function of r.

Fig. 3 shows V/N, $A^{(d=3)}/N$, H/N and $\chi^{(d=3)}/N$ as a function of r for one single configuration of a random point set with $N = 1024$ and $L_x = 128$ ($\rho = 0.00049$). The dotted (dashed) lines show the data for periodic (free)

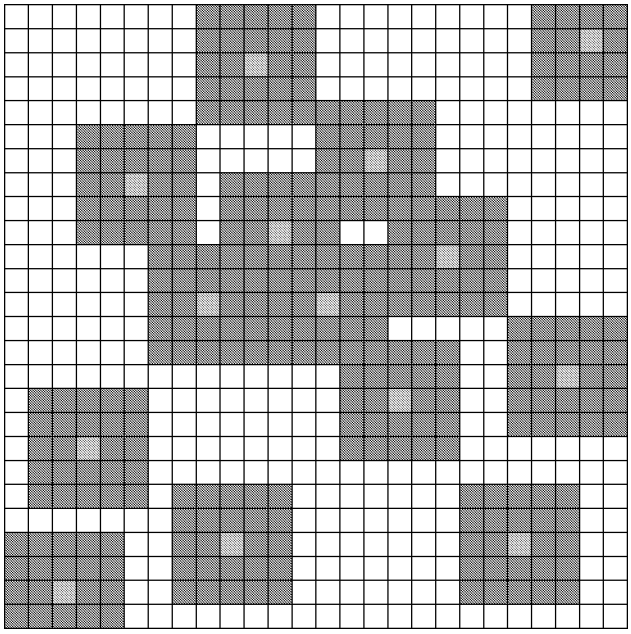

Fig. 2. Graining procedure of a point pattern in two dimensions. The grains are squares of edge length $2r+1=5$. The light grey pixels indicate the positions of the germs. In MIA all dark pixels are considered to be black.

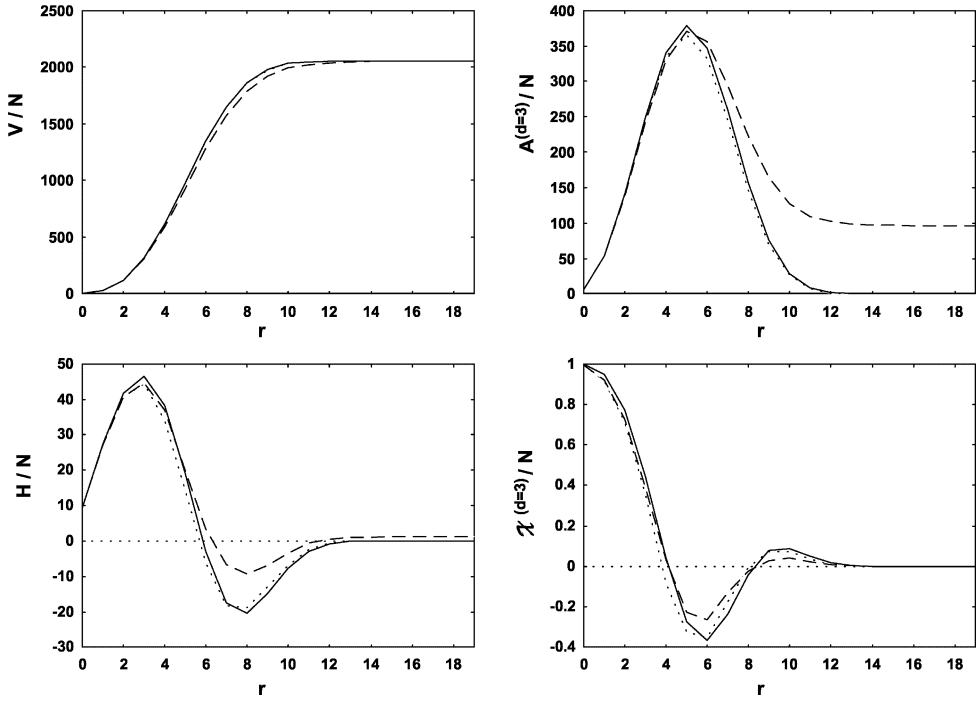

Fig. 3. Morphological quantities as a function of r for a random point set in a cubic box with cubic grains centered around each point. The cubic box has edge length $L_x=128$ and contains $N=1024$ germs. Dotted lines: periodic boundary conditions, dashed lines: free boundary conditions, solid lines: results obtained from discrete integral geometry (see (10)).

boundary conditions. The solid lines are the results obtained from (10). For small r the grains are isolated leading to a small covered volume and surface area and to a positive integral mean curvature and Euler characteristic. For large r the grains largely overlap and cover almost completely the whole cube. Only small cavities remain. This gives rise to a large covered volume which approaches L_x^3 in the case of the completely covered cube. The surface area and integral mean curvature are small and approach zero ($6L_x^2$) and zero ($3\pi L_x$), respectively for a completely covered cube with periodic (free) boundary conditions. For large r the Euler characteristic is positive and approaches 0 (1) in the case of the completely covered cube with periodic (free) boundaries. For intermediate r the coverage has a tunnel-like structure with a negative Euler characteristic and a large surface area. The integral mean curvature changes sign in the regime of intermediate r. For periodic boundary conditions (dotted lines) there is an excellent agreement between the numerical data and the theoretical result (10). For free boundary conditions (dashed lines) the agreement is less good especially for the case of the surface area and the integral mean curvature.

In Fig. 4 we depict $A^{(d=2)}/N$, L/N and $\chi^{(d=2)}/N$ as a function of r for one single configuration of a random point set with $N = 10\,240$ and $L_x = 1024$ ($\rho = 0.0098$). The dotted (dashed) lines show the data for periodic (free) boundary conditions. The solid lines are the results obtained from (11). Also in this case there is excellent agreement between the numerical data for periodic and free boundary conditions and the theoretical result (11). Note that for both $d = 2$ and $d = 3$ the agreement is remarkable as only one realization of a random point set was used in the simulation.

The simulation results shown in Figs. 3 and 4 have been obtained by using one realization of random points. Repeating these simulations with different realizations yields figures that cannot be distinguished from those shown in Figs. 3 and 4. In the limit $r \to \infty$, where the whole box is filled with black voxels, the surface area of the box

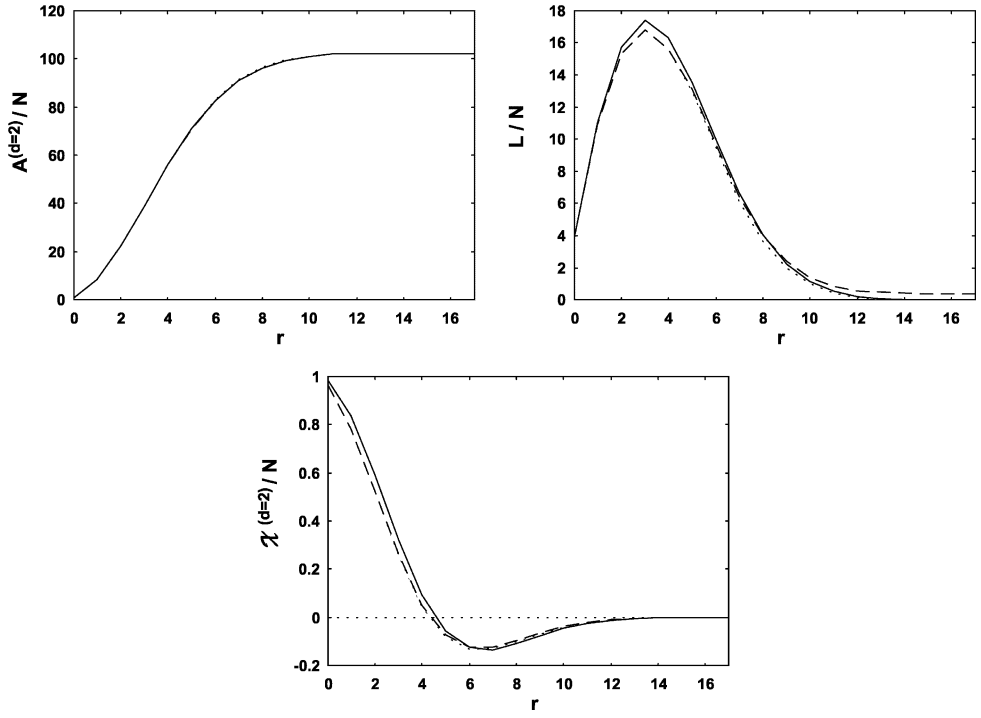

Fig. 4. Morphological quantities as a function of r for a random point set in a square region with square grains centered around each point. The square region has edge length $L_x = 1024$ and contains $N = 10\,240$ germs. Dotted lines: periodic boundary conditions; dashed lines: free boundary conditions; solid lines: results obtained from discrete integral geometry (see (11)).

with free (periodic) boundary conditions approaches $6L_x^2$ (0). This shows that in MIA the differences between data for free and periodic boundary conditions cannot be taken as a measure for finite-size effects.

4. Summary

We have described a morphological image analysis (MIA) method to characterize black-and-white images in terms of shape (geometry) and connectivity (topology). Integral-geometry-based MIA allows a straightforward calculation of the morphological quantities and requires little computational effort. The approach has been illustrated by computation of the morphological measures of random point sets on a cubic lattice. MIA is easy to use. Results of applications to perfect and imperfect SC, FCC and BCC lattice structures, to triply periodic minimal surfaces and to three-dimensional structures formed in polymer solutions will be published elsewhere [6,8].

Acknowledgements

We are grateful to Prof. H. Wagner for very helpful advice. Part of this research has been financially supported by the Council for Chemical Sciences of the Netherlands (CW/NWO) and Unilever Research Laboratories.

Appendix A. Example

```
!!!!!!!!!!!!!!!!!!!!!!!!!!!!!!!!!!!!!!!!!!!!!!!!!!!!!!!!!!!!!!!!!!!!!!!!
!                                                                      !
!  Mink_3D_free computes the change of the Minkowski functionals      !
!  (volume,surface,curvature,euler3D) if a pixel is added to the 3D   !
!  image contained in the 1D array LATTICE. A pixel at position       !
!  x=jx+Lx*(jy+Ly*jz) is active (black) if LATTICE(x)=1, otherwise    !
!  LATTICE(x)=0. Active pixels should only appear at positions        !
!  (0 < jx < Lx, 0 < jy < Ly, and 0 < jz < Lz).                       !
!  Pixels at the boundary of LATTICE should be zero in order to       !
!  correctly implement free boundary conditions.                      !
!                                                                      !
!!!!!!!!!!!!!!!!!!!!!!!!!!!!!!!!!!!!!!!!!!!!!!!!!!!!!!!!!!!!!!!!!!!!!!!!
        implicit integer (a-z)
        integer lattice(0:LX*LY*Lz-1)
        parameter(
     1   volume_body=1   ,      !(a*a*a, where a is lattice displacement)
     1   surface_body=-6 ,       !(-6*a*a, open body)
     1   surface_face=2  ,       !(2*a*a, open face)
     1   curv_body=3     ,       !(3*a, open body)
     1   curv_face=-2    ,       !(-2*a, open face)
     1   curv_edge=1     ,       !(a, open line)
     1   euler3D_body=-1 ,       !(open body)
     1   euler3D_face=1  ,       !(open face)
     1   euler3D_edge=-1 ,       !(open line)
     1   euler3D_vertex=1)       !(vertices)
```

```
      nfaces=0
      nedges=0
      nvert=0

      do i=-1,1,2
      jxi=jx+i
      jyi=jy+i
      jzi=jz+i
      kc1=1-lattice(jxi+Lx*(jy+Ly*jz))
      kc2=1-lattice(jx+Lx*(jyi+Ly*jz))
      kc3=1-lattice(jx+Lx*(jy+Ly*jzi))
      nfaces=nfaces+kc1+kc2+kc3
      do j=-1,1,2
      jyj=jy+j
      jzj=jz+j
      k4=Lx*(jyj+Ly*jz)
      k7=Lx*(jy+Ly*jzj)
      kc7=1-lattice(jx+k7)
      kc1kc4kc5=kc1*(1-lattice(jxi+k4))*(1-lattice(jx+k4))
      nedges=nedges+kc1kc4kc5+kc2*(1-lattice(jx+Lx*(jyi+Ly*jzj)))*kc7
     1                        +kc1*(1-lattice(jxi+k7))*kc7
      if(kc1kc4kc5.ne.0) then
      do k=-1,1,2
      jzk=jz+k
      k9=Lx*(jy+Ly*jzk)
      k10=Lx*(jyj+Ly*jzk)
      nvert=nvert+(1-lattice(jxi+k9))*(1-lattice(jxi+k10))
     1              *(1-lattice(jx+k10))*(1-lattice(jx+k9))
      enddo ! k
      endif ! kc1kc4kc5
      enddo ! j
      enddo ! i

      volume=volume\_body
      surface=surface\_body+surface\_face*nfaces
      curvature=curv\_body+curv\_face*nfaces+curv\_edge*nedges
      euler3D=euler3D\_body+euler3D\_face*nfaces
     1          +euler3D\_edge*nedges+euler3D\_vertex*nvert

      end
```

References

[1] A. Rosenfeld, A.C. Kak, Digital Picture Processing (Academic Press, New York, 1982).
[2] H. Hadwiger, Vorlesungen über Inhalt, Oberfläche und Isoperimetrie (Springer Verlag, Berlin, 1957).
[3] L.A. Santaló, Integral Geometry and Geometric Probability (Addison-Wesley, Reading, MA, 1976).
[4] D. Stoyan, W.S. Kendall, J. Mecke, Stochastic Geometry and its Applications (Akademie Verlag, Berlin, 1989).

[5] K.R. Mecke, Int. J. Mod. Phys. B 12 (1998) 861 and references therein.
[6] K. Michielsen, H. De Raedt, submitted to Physics Reports.
[7] G. Matheron, Random Sets and Integral Geometry (John Wiley and Sons, New York, 1975).
[8] K. Michielsen, H. De Raedt, J.G.E.M. Fraaije, Prog. Theor. Phys. (in press).